Thin-Walled Structures 47 (2009) 637–645

Contents lists available at ScienceDirect

Thin-Walled Structures

journal homepage: www.elsevier.com/locate/tws

Plastic collapse analysis of thin-walled circular tubes subjected to bending

S. Poonaya *, U. Teeboonma, C. Thinvongpituk

Department of Mechanical Engineering, Faculty of Engineering, Ubonratchathani University, Warinchamrap Ubonratchathani 34190, Thailand

ARTICLE INFO

Article history:
Received 15 May 2008
Received in revised form
7 November 2008
Accepted 7 November 2008
Available online 18 January 2009

Keywords:
Bending
Circular tube
Collapse mechanism
Energy absorber

ABSTRACT

Circular tubes have been widely used as structural members in many engineering applications. Therefore, its collapse behavior has been studied for many decades, focusing on its energy absorption characteristics and collapse mechanism. In order to predict the collapse behavior of members, one could rely on the use of finite element codes or experiments. These tools are helpful and have high accuracy but are costly and require extensive running time. Therefore, an approximate model of tubes collapse mechanism is an alternative especially for the early step of design. This paper is also aimed to develop a closed-form solution to predict the moment–rotation response of circular tube subjected to pure bending. The model was derived based on the principle of energy rate conservation. The collapse mechanism was divided into three phases. New analytical model of ovalisation plateau in phase 2 was derived to determine the ultimate moment. In phase 3, the Elchalakani et al. model [Int. J. Mech. Sci. 2002; 44:1117–1143] was developed to include the rate of energy dissipation on rolling hinge in the circumferential direction. The 3-D geometrical collapse mechanism was analyzed by adding the oblique hinge lines along the longitudinal tube within the length of the plastically deformed zone. Then, the rates of internal energy dissipation were calculated for each of the hinge lines which were defined in terms of velocity field. Inextensional deformation and perfect plastic material behavior were assumed in the derivation of deformation energy rate. In order to compare, the experiment was conducted with a number of tubes having various D/t ratios. Good agreement was found between the theoretical prediction and experimental results.

© 2008 Elsevier Ltd. All rights reserved.

1. Introduction

Many researchers have been investigating the collapse mechanism and energy absorption capacity of many structures, majority focusing on thin-walled structures such as shell, tubes, stiffeners and stiffened sandwich panels. These structures have been identified as a very efficient impact energy absorbing system and called "energy absorber". The study of deformation in the energy absorber accounts for various parameters such as geometrical shape, mode of collapse, strain hardening and strain rate effect. In general, there are several approaches to determine the energy absorption of structural members, by using finite element analysis, experiments and theoretical analysis. Although finite element analysis and experimental approaches can provide accurate results, they are costly and require extensive running time. Therefore, the theoretical analysis is an alternative for the early step of design.

Theoretical analysis of the collapse can be made by using the hinge line method. When thin-walled members are crushed by any load, the collapse strength is reached. Then, plastic deformations occur over some folding lines and these are called "hinge lines". When hinge lines are completed around the structure, global or local collapse will progress. The internal energy in deformed structure is determined by the summation of plastic energy dissipated in each hinge line.

Many researchers have studied the plastic collapse behavior and energy absorption characteristics of thin-walled tubes subjected to bending. Kecman [1], studied the deep bending collapse of thin-walled rectangular columns and proposed a simple failure mechanism consisting of stationary and rolling plastic hinge line. The analytical solution was achieved using limit analysis techniques. Zhang and Yu [2] studied the ovalisation of a tube with an arbitrary cross section and one symmetric plane to obtain a full moment–curvature response. Their analysis showed that the flattening increases nonlinearly as the longitudinal curvature increases up to a limiting maximum value. Wierzbicki and Bhat [3] derived a closed-form solution to predict the pressure necessary to initiate and propagate a moving hinge on the tube. The calculations were performed using a rigid–plastic material, and a simple moving hinge model was assumed to occur along the hinge line. The deformation of a ring was modeled into a "dumbbell" shape. The analytical results agreed well with the experiments. Wierzbicki and Suh [4], conducted a theoretical analysis of the large plastic deformations of tubes subjected to

* Corresponding author.
E-mail address: s_poonaya@yahoo.co.th (S. Poonaya).

0263-8231/$ - see front matter © 2008 Elsevier Ltd. All rights reserved.
doi:10.1016/j.tws.2008.11.005

combined load in the form of lateral indentation, bending moment and axial force. The model was effectively decoupling the 2-D problem into a set of 1-D problems. The theoretical results gave good correlation with existing experimental data. Cimpoeru and Murray [5] presented empirical equations of the moment–rotation relation of a square thin-walled tube subjected to pure bending where the width-to-thickness ratio was less than 26. Results from the empirical model were compared with the analytical model of Kecman [1]. Wierzbicki et al. [6] studied the bending collapse mechanism of thin-walled prismatic columns by the concept of basic folding mode. They developed the collapse mechanism by adding the toroidal and rolling deformation in the compressive model. Close-form solutions were derived for the moment–rotation characteristic of square column in the post failure range. The stress profiles in the most general case of a floating neutral axis were also shown. The simplified analytical solution was used to predict the moment–rotation relationship with an absolute error not greater than 7%. Wiezbriki and Sinmao [7] studied the simplified model of circular tube in pure bending, which was valid for large and very large sectional distortion. Good agreement with numerical solution (ABAQUS) was obtained. Kim and Reid [8] modified the mechanism model of Wierzbicki et al. [6], and suggested that the toroidal deformation and conical rolling should be defined differently from the case of axial compression to satisfy the bending kinematics condition. Good agreement was found between the model and the experiment. Elchalakani et al. [9] predicted the response of a circular steel tube under pure bending. They included the effect of ovalisation along the length of the tube into the model. Work dissipated through the toroidal and the rolling hinges was ignored. The hinge mechanism was assumed straight and inextensible. Good agreement between analytical result and experiment was achieved. In another report, Elchalakani et al. [10] presented a closed-form solution of the post-bucking collapse of the slender circular hollow section with $D/t>85$ subjected to pure bending. The theoretical analysis closely matched with the experimental results.

The main objective of this paper is to develop a close-form solution of thin-walled circular tube subjected to bending using a rigid plastic mechanism analysis. The model of ovalisation phase is derived to determine the ultimate moment. In addition to the structural collapse phase, Elchalakani's model [9] is developed to include the rate of energy dissipation of rolling hinge in the circumferential direction. The model is based on the principle of energy rate conservation and is analyzed in the 3-D problem by adding the longitudinal hinges in plastic zone. The theoretical model is presented and then resolved in the form of moment–rotation characteristics.

2. Theoretical predictions

In general, the collapse mechanism of tube subjected to bending can be divided into three phases, elastic behavior, ovalisation plateau and structural collapse. Each phase behaves in a different deformation mode. The present study attempted to develop the collapse model of each phase by focusing on their moment–rotation relationship individually. The analytical model of each phase is derived as explained.

2.1. Elastic behavior

In this phase, the moment increases linearly with constant slope up to a yield moment–rotation. The elementary theory of elasticity is generally used to predict the linear moment–rotation characteristic of a circular tube. Yield moment and the corresponding angle are defined by

$$M_y = \frac{2\sigma_y I}{D_o} \tag{1}$$

$$\theta_y = \frac{M_y L_0}{EI} \tag{2}$$

where M_y is the yield moment, L_0 is the moment length, E is the elastic modulus, I is the second moment of area, σ_y is the measured yield stress, θ_y is the yield rotation angle and D_o is the outside diameter of the tube.

2.2. Ovalisation plateau

In phase 2, the circular cross section of tube subjected to bending started to deform in an oval shape. In general, the bending moment in this phase is assumed constant and ultimate. Ueda [11] derived the moment–rotation relationship by considering the strains developed at the surface of the tube under constant moment. He assumed that an initially circular cross section is deformed to an elliptical cross section. The ultimate bending moment was obtained by integrating stress over the cross section. His ultimate moment is expressed as

$$M_u = \sigma_y Z_p + (\sigma_u - \sigma_y) Z_e \tag{3}$$

where σ_y is the yield stress, σ_u is the ultimate tensile stress, $Z_p = (4/3)(R_o{}^3 - R_i{}^3)$ is the plastic bending section modulus, $Z_e = (\pi/4R_o)(R_o{}^4 - R_i{}^4)$ is the elastic bending section modulus, R_o is the outer radius of tube, and R_i is the inner radius of tube.

Recently, Elchalakani et al. [12,13] also determined the ultimate moment of circular hollow section by approximating the ovalised section as an elliptical shape. Their experiments suggested that the ovalisation starts when the major axis reaches $1.10d$ and the minor axis reaches $0.9d$. The solution for their ultimate moment is shown in the following equation:

$$M_u = S_{ovalised}\sigma_y = \frac{4}{3}(R_v^2 R_h - R_{vi}^2 R_{hi})\sigma_y \tag{4}$$

where $S_{ovalised}$ is the plastic section modulus of an ovalised tube, σ_y is the measured yield stress of an ovalised tube. $R_h = D_h/2 = 0.55D_o$ and $R_v = D_v/2 = 0.45D_o$ are the external horizontal and vertical radii of an ovalised tube, respectively. The internal horizontal and vertical radii are $R_{hi} = (R_h - t)$ and $R_{vi} = (R_v - t)$, respectively, and t is the thickness of tube.

The present paper aims to propose a new model for sectional ovalisation by developing the model of those two works [11,12]. The new ovalisation model proposed here is shown in Fig. 1. The radius of curvature R_1 which is formed at both ends of flattening

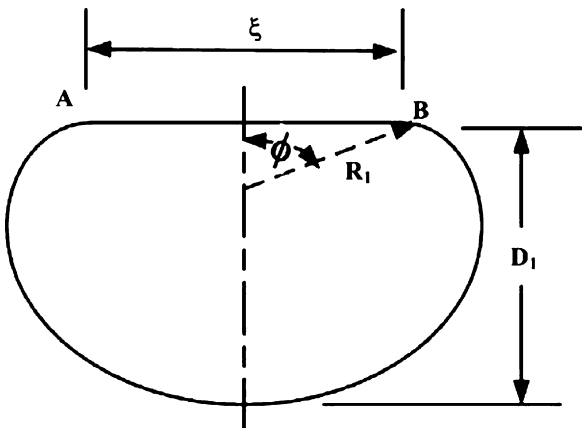

Fig. 1. The proposed model of ovalisation of tube due to bending.

sides is taken into account. Although the behavior of material exhibits as slight hardening, the bending moment is assumed constant during the increment of bending rotation. The rolling hinge of the circumferential cross section is ignored. Then, the ultimate moment of an ovalised tube and the corresponding angle of rotation are determined by integrating the stress over the cross section.

From Fig. 1, the geometry of circumferential cross section of tube is assumed inextensible and can be expressed as

$$\frac{\xi}{2} + R_1(\pi - \phi) = \pi R \tag{5}$$

where $\xi/2 = R_1 \sin(\phi)$ and R is the initial radius of the tube.

The bending moment in a tube can be obtained by integrating the stress over the circumferential cross section which is expressed as

$$M = \int_A \sigma z \, dA \tag{6}$$

where $dA = t\,ds$ is the cross-sectional area of an element of the tube, t is the thickness of the tube, z is the distance from the neutral axis of a sectional ovalisation to the circumferential area and ds is the length of the circumferential cross section.

By integrating Eq. (6), the expression for moment can be obtained as

$$M = 2\sigma_0 t \int_0^{\pi R} z\, ds$$
$$M = \sigma_0 t R_1^2(\sin(2\phi) + 2\,\sin(\phi)) \tag{7}$$

where $R_1 = \pi R/(\pi - \phi + \sin(\phi))$, for large deformation the R_1 is equal to the outside radius of tube, R.

The ultimate bending moment can be determined by minimizing the bending moment in Eq. (7) with respect to the deformation angle ϕ. The ultimate bending moment is finally obtained as

$$M_u = 3\sigma_0 t R^2 \tag{8}$$

where σ_0 is the ultimate stress of material, t is the thickness of the tube, and R is the outside radius of the tube.

The changing angle of rotation between phase 1 (elastic regime) and phase 2 (ovalisation regime) is determined by

$$\theta_{oval} = \frac{M_u}{EI} \tag{9}$$

where M_u is the ultimate moment obtained from Eq. (8), E is the elastic modulus, and I is the second moment of area.

The rotation angle at the end of phase 2 is, still, cannot be determined theoretically. However, this study assumes the intersection between the moment–rotation angle curves of phase 2 and phase 3 to be the end angle of phase 2 and, hence, to be the onset angle of phase 3.

2.3. Structural collapse

In phase 3, the structure starts to collapse resulting in load carrying capacity to decrease rapidly. The present paper proposes a modified collapse model as shown in Fig. 2. The model involves the flattened hinge (AB) in the circumferential cross section and the oblique hinge lines along the longitudinal direction of tube (AS and BS), as shown in Figs. 2(a) and (c), respectively.

The traveling hinges of the flattened region in the circumferential cross section in Fig. 2(a) are modeled as a line connecting points A and B. The rolling hinge has radius r and circular arc of current radius R_1. Figs. 2(b) and (c) show the deformation of four oblique hinge lines along the longitudinal tube within the length of plastic zone H.

2.3.1. Assumptions

In order to analyze the proposed collapse model in Fig. 2, the following assumptions were made:

1. The tube material is ductile, rigid–perfectly plastic, isentropic, homogeneous and material compatibility condition is maintained.
2. The tube circumference is inextensible.
3. Shear deformation and twist of the deformed tube are neglected.

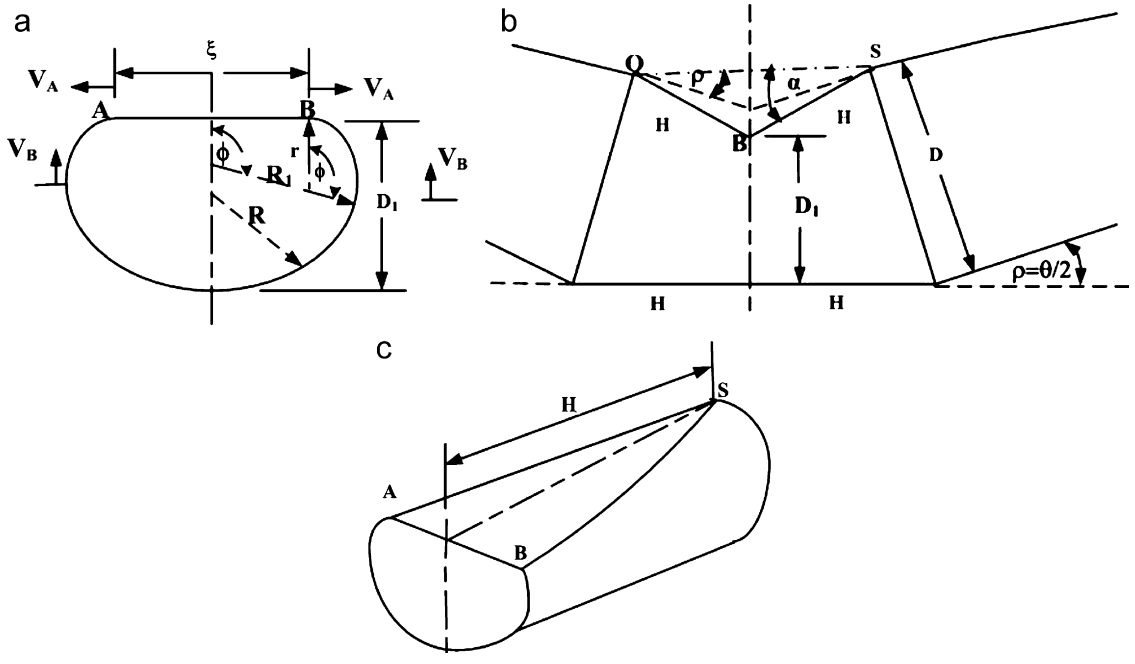

Fig. 2. Plastic collapse model of thin-walled circular tube subjected to pure bending.

4. The collapse mechanism formed in the tube is kinematically admissible and the cross section of the tube deforms in a simplified manner as shown in Fig. 2.
5. All hinges are assumed straight. Work dissipation through the toroidal region is ignored, but the rolling hinges in the deformed cross section are considered.
6. The initial mean radius of tube (R) is the tube's cross-section radius at the beginning of the plastic hinge formation.
7. The tube does not elongate or contract in the axial direction.
8. The radius R_1 is constant and equal to the outside radius of tube (R) during large deformation of the cross section.
9. The parameter H and r are constant during the collapse of section.

2.3.2. Geometrical analysis

From the kinematics of the collapse mechanism shown in Fig. 2, the global geometry of collapse can be expressed as

$$\xi + r\phi + R_1 = (\pi R) \tag{10}$$

where R is the mean radius of circular tube, R_1 is the radius of deformed cross section, ξ is the length of hinge line ((AB) in Fig. 2(a)), and ϕ is the mechanism angle defined in Fig. 2(a).

The vertical displacement D_1 of circular cross section, in Fig. 2(a) is defined by

$$D_1 = R_1(1 + \cos\,\phi) + r(1 - \cos\,\phi) \tag{11}$$

and in Fig. 2(b) by

$$D_1 = 2R\cos\,\rho - H\sin\,\alpha \tag{12}$$

where $\alpha = (\pi/2) - \arcsin(1-(2R/H)\sin\rho)$, $\rho = \theta/2$, and θ is the bending rotation at the end of the tube.

Thus, the relationship between the mechanism angle ϕ and the bending angle ρ can be determined from Eqs. (11) and (12) using the numerical techniques and can be expressed as

$$\phi = \frac{[4(RH)^{1/2}\rho^{1/2}]^{1/2}}{(R-r)^{1/2}} \tag{13}$$

The velocity of hinge propagation, in Fig. 2(a) is expressed as

$$V_A = \frac{d\xi}{dt} = \dot{\xi} \quad \text{and} \quad V_B = \frac{dR_1(\pi-\phi)}{dt} = -R_1\dot{\phi} \tag{14}$$

2.3.3. Plastic energy dissipation

The rate of internal energy dissipation resulting from continuous and discontinuous deformation rate fields is defined by

$$\dot{E} = \int_S (M_{\alpha\beta}\dot{\kappa}_{\alpha\beta} + N_{\alpha\beta}\dot{\varepsilon}_{\alpha\beta})\,dS + \sum_{i-1}^{n}\int_{l^i} M_n^i[\dot{\psi}_i]\,dl^i \tag{15}$$

where S denotes the current shell midsurface, n is the total number of plastic hinge lines, l^i is the length of the ith hinge, and $[\dot{\psi}_i]$ denotes a jump of the rate of rotation across the moving hinge line. The components of the rate of rotation and the rate of extension tensors are denoted by $\dot{K}_{\alpha\beta}$ and $\dot{\varepsilon}_{\alpha\beta}$, respectively. The corresponding conjugate generalized stresses are the bending moment $M_{\alpha\beta}$ and the membrane forces $N_{\alpha\beta}$. $M_n = (2/\sqrt{3})(\sigma_o t^2/4)$ is the plane strain plastic bending moment (per unit length) normal to the hinge line. All components are expressed in the cylindrical coordinate system on the surface of the shell.

There are six important components in the first integration term of Eq. (15); i.e., $\dot{\varepsilon}_{xx}$, $\dot{\varepsilon}_{x\theta}$, $\dot{\varepsilon}_{\theta\theta}$, $\dot{K}_{xx}$, $\dot{K}_{x\theta}$, and $\dot{K}_{\theta\theta}$. Each of these components will be considered individually.

Regarding the assumption that shear deformation and twist of the deformed shell are neglected, we have $\dot{\varepsilon}_{\alpha\theta} = \dot{K}_{\alpha\beta} = 0$. The tube circumference is inextensible, hence $\dot{\varepsilon}_{\theta\theta} = 0$. Later, the local change in the axial curvature is assumed to be small compared to the change in the circumferential curvature, resulting in $\dot{K}_{xx} < \dot{K}_{\theta\theta}$, and thus $\dot{K}_{xx}$ will be neglected. Finally, the axial strain rate is zero, $\dot{\varepsilon}_{xx} = 0$, due to Assumption 7 as explained in Section 2.3.1. Hence, the expression for the rate of internal energy dissipation expressed in Eq. (15) can be reduced to

$$\dot{E} = \int_s (N_{xx}\dot{\varepsilon}_{xx} + M_{\theta\theta}\dot{\kappa}_{\theta\theta})\,ds + \sum_{i=1}^{n}\int_{L^i} M_n^i[\dot{\psi}_i]\,dl^i \tag{16}$$

Eq. (16) is the governing equation that will be used to calculate energy dissipation in plastic hinges. The individual plastic hinge is analyzed as follows.

2.3.3.1. Rate of lateral crushing energy of the tube. The expression for the rate of energy of shape distortion or lateral crushing of tube can be derived from Eq. (16) and is obtained as

$$\dot{E}_{crush} = \int_s (M_{\theta\theta}\dot{\kappa}_{\theta\theta})\,ds + \sum_{i=1}^{n}\int_{L^i} M_n^i[\dot{\psi}_i]\,dl^i \tag{17}$$

where the plastic bending moment $M_{\theta\theta} = \sigma_{\theta\theta}t^2/4$, $\sigma_{\theta\theta}$ is the circumferential stress and t is the thickness of the tube. The rates of curvature, $(\dot{\kappa}_{\theta\theta})$ along the straight flattened length $(\dot{\kappa}_{\theta\theta})_A$ and around the semi-circular curve are defined by

$$(\dot{\kappa}_{\theta\theta})_A = -\frac{\dot{R}_1}{R_1^2} \quad \text{and} \quad (\dot{\kappa}_{\theta\theta})_B = -\frac{\dot{r}}{r^2} \tag{18}$$

Since the rolling hinge, r and R_1 are assumed constant along the rotational angle θ, the rate of curvature is equal to zero, $(\dot{\kappa}_{\theta\theta}) = 0$.

By using the assumptions and geometrical analysis explained earlier, the rate of lateral crushing energy dissipated in the tube can be derived as follows:

$$\dot{E}_{crush} = \sum_{i=1}^{n}\int_{L^i} M_n^i[\dot{\psi}_i]\,dl^i \tag{19}$$

where M_n is the bending moment normal to the hinge line, and the rate of rotation $\dot{\psi}$ at the moving hinge line is calculated from the condition of kinemetic continuity

$$\dot{\psi} = V[K] \tag{20}$$

where V is the velocity of the traveling hinge in the tangential direction and K is the circumferential curvature. $[K] = K^+ - K^-$ is the jump in curvature from either side of the hinge line. Ahead of the hinge $K^+ = 1/r$ and behind the hinge $K^- = 0$ (flat sections), the rate of rotation at the hinge is

$$\dot{\psi}_A = V_A\left[\frac{1}{r}\right] \quad \text{and} \quad \dot{\psi}_B = V_B\left[\frac{1}{r} - \frac{1}{R_1}\right] \tag{21}$$

where V_A and V_B are tangential velocities in the current deformed configuration of the ring in Fig. 2(a) and are given by

$$V_A = \frac{d\xi}{dt} = \dot{\xi}, \quad V_B = \frac{-dR_1(\pi-\phi)}{dt} \tag{22}$$

The bending moment normal to the hinge line (M_n) is assumed to be equal to the circumferential bending moment ($M_{\theta\theta}$) on the continuous deformation region, $M_n = M_{\theta\theta} = (\sigma_{\theta\theta}t^2/4)$.

An approximate yield condition for the present problem is given by

$$\left(\frac{M_{\theta\theta}}{M_0}\right)^2 + \left(\frac{N_{xx}}{N_0}\right)^2 = 1 \tag{23}$$

The plastic compressive-tensile stress (σ_{xx}) in axial direction resulting from bending is coupled with bending-induced hoop stress ($\sigma_{\theta\theta}$) through an inscribed yield condition, to one point with the coordinate,

$$\frac{\sigma_{\theta\theta}}{\sigma_0} = \frac{M_{\theta\theta}}{M_0} = \frac{1}{\sqrt{2}}, \quad \frac{\sigma_{xx}}{\sigma_0} = \frac{N_{xx}}{N_0} = \frac{1}{\sqrt{2}} \tag{24}$$

The rate of energy dissipation in the crushing mode can be rewritten by substituting Eqs. (18), (21), (22) and (24) in Eq. (19): for full cross section of tube,

$$\dot{E}_{crush} = \frac{M_0 t}{8\sqrt{2}R^2} H\left((R_1 - r)\cos\phi\left[\frac{1}{r}\right] + R_1\left[\frac{1}{r} - \frac{1}{R_1}\right]\right)\dot{\phi} \tag{25}$$

where $M_0 = \int_A \sigma_0 z\, dA = 4\sigma_0 R^2 t$ is the fully plastic bending moment of the undeformed cross section [7].

2.3.3.2. Rate of energy dissipation over the central hinge AB. Energy dissipated in the central hinge line (AB) can be expressed as shown in Eq. (26). Its length depends on the angle α:

$$\dot{E}_{AB} = \sum_i M_n l_i \dot{\psi}_i = \frac{\mathrm{M}_0 t}{8\sqrt{2}R^2}(\xi)\dot{\alpha} \tag{26}$$

where i is the number of hinge lines, $l_i = \xi$ is the length of hinge line, $\dot{\psi} = 2\dot{\alpha}$ is the rate of rotation angle of hinge lines, and $\dot{\alpha}$ can be determined from Eq. (10).

2.3.3.3. Rate of energy dissipation over the oblique hinge lines SA, SB, OA, and OB. The plastic energy dissipated over four oblique hinge lines SA, SB, OA, and OB, as shown in Fig. 2(b) and (c) can be calculated by using the following expression:

$$\dot{E}_{OB} = \sum_i M_n l_i \dot{\psi}_i = \frac{M_0 t}{4\sqrt{2}R^2}\dot{\xi} \tag{27}$$

where $i = 4$ is the number of hinge lines, $l_h = \sqrt{H^2 + \xi^2}$ is the length of each hinge line, and $\dot{\psi} = V_A/l_h = \dot{\xi}/l_h$ is the rate of rotation angle of each hinge line. $\dot{\psi}$ is assumed to vary along the tangential velocity V_A of the moving hinge AB and $\dot{\xi} = 2(R_1 - r)\cos(\phi)\dot{\phi}$.

2.3.3.4. Instantaneous moment. The global energy balance of a single structural element can be established by equating the rate of energy dissipation and the rate of external work.

$$\dot{E}_{ext} = \dot{E}_{\mathrm{int}} \tag{28}$$

where $\dot{E}_{ext}$ is the rate of external work, and $\dot{E}_{\mathrm{int}}$ is the internal rate of energy dissipation at the plastically deformed region.

The rate of total internal energy dissipation $\dot{E}_{\mathrm{int}}$ is defined by

$$\dot{E}_{\mathrm{int}} = \dot{E}_{crush} + \dot{E}_{AB} + \dot{E}_{OB} \tag{29}$$

External rate of energy dissipation is defined by

$$\dot{E}_{ext} = M\dot{\theta} \tag{30}$$

The instantaneous moment can be determined by substituting all expressions for plastic energy into Eq. (29) and substituting Eq. (30) in Eq. (28), finally the corresponding moment is obtained as a function of H, r, and θ:

$$M = M(H, r, \theta) \tag{31}$$

The mean crushing moment (M_m) can be determined by integrating moment (M) in Eq. (31) with respect to the rotation angle from $\rho = 0$ to $\rho = \rho_f(H)$:

$$M_m(H, r) = \frac{1}{\rho_f}\int_0^{\rho_f(H)} M\, d\rho \tag{32}$$

where $\rho_f(H)$ is the contact angle where the upper and lower sections gets in contact. This angle can be determined by defining term D_1 in Eq. (12) equal to zero and hence

$$\rho_f(H) = \cos^{-1}\left(\frac{R}{H}\right) \tag{33}$$

Similarly the mechanism angle of final collapse ϕ_f is obtained from Eq. (13) by defining term $D_1 = 0$. Hence, ϕ_f is obtained as

$$\phi_f = \frac{2}{(R - r)}[(R - r)R]^{1/2} \tag{34}$$

The length of the plastic folding region (H) and the rolling radius (r) can be determined from the postulate of minimum mean crushing moment in Eq. (32). Then, the solution can be expressed as

$$H = 1.31R \quad \text{and} \quad r = 0.6R \tag{35}$$

The value of H and r are then substituted into Eq. (31) to give the expression for the instantaneous moment in terms of the rotation angle θ:

$$M = M(\theta) \tag{36}$$

Details of each moment component are presented in the Appendix.

3. Experiments

3.1. Specimen preparation

In order to verify the proposed model, the experiment was conducted with 18 tubes. These tubes were divided into 6 groups, each group consisted of 3 cold formed mild steel tubes with similar geometries. The nominal diameter-to-thickness ratios range from 21.16 to 42.57 and the length of each specimen is 1500 mm. The material properties were determined by using the tensile coupons tested according to the British Standard BSEN 10 002-1:1990 [14]. Results from tensile tests are shown in Table 1. It is observed from Table 1 that the value of modulus of elasticity of UB1, UB5, and UB6 are a bit low compared to other specimens. This is due to the variation of material property in the local market. However, this does not affect the study results because the comparisons of experimental and analytical results were based on each corresponding material.

3.2. Test setup and procedure

The experimental setup was designed to obtain a pure bending moment over middle span of the specimen. The influence of shear and axial forces should be avoided or minimized as much as possible. To meet this requirement, Cimpoeru et al. [5] introduced a machine that is able to apply a pure bending moment without imposing shear or axial forces. A machine based on that concept has been built at Ubonratchathani University to apply a pure bending test on those 18 specimens. The diagram of this machine is shown in Fig. 3.

As can be seen from the diagram in Fig. 3, the machine consists of two load application wheels on its left and right ends. These two wheels are connected to the tensile testing machine via two connecting rods. The tested tube is placed on the load application wheels and locked with two bolts on each side. As the tensile machine pulls the connecting rods upward, the wheels start to rotate and apply pure bending moment on the tested specimen. Fig. 4 shows an experimental setup and various views of deformed specimen. The experimental collapse mode was found similar to the proposed model shown in Fig. 2.

4. Results and discussions

Two main findings of this paper are the ultimate moment which was analyzed from the ovalisation regime and the model of

Table 1
Dimensions and material properties of specimens..

Specimen no.	Diameter (mm)	Thickness (mm)	D/t	Modulus of elasticity, E (GPa)	Yield stress, σ_y (MPa)	Ultimate stress, σ_u (MPa)	Yield angle, θ_y (deg.)	Yield moment, M_y (kN m)
UB1	59.25	2.80	21.16	128	330	383	2.99	2.21
UB2	59.00	2.30	25.65	160	270	314	1.96	1.51
UB3	46.85	1.80	26.03	173	320	355	3.17	1.01
UB4	59.35	1.80	32.97	178	354	370	2.30	1.61
UB5	58.55	1.60	36.59	128	257	295	2.44	1.02
UB6	74.50	1.75	42.57	133	306	380	2.41	2.45

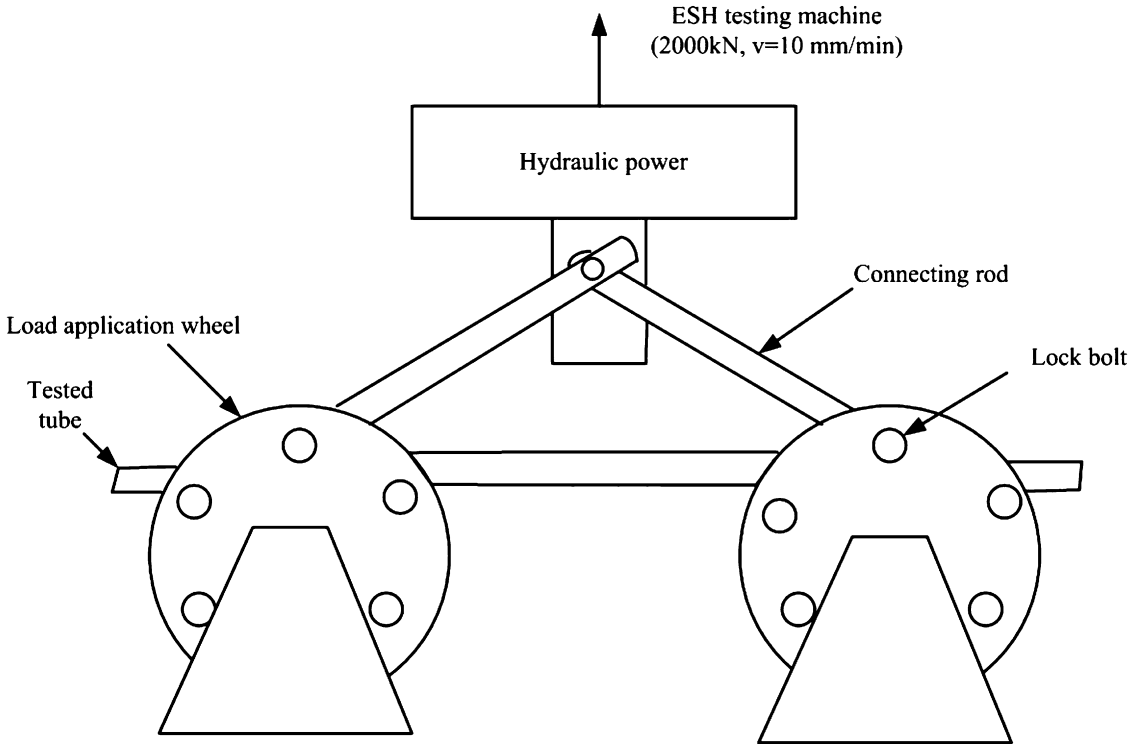

Fig. 3. The diagram of the pure bending machine used in this study.

plastic collapse in the structural collapse regime. The results and their discussions are presented below.

4.1. The comparison of ultimate moment with experimental results and other simplified models

The ultimate moment analyzed in this paper are compared with experimental results as well as with available models such as Ueda's [11] and Elchalakani's [12]. Table 2 shows a summary of the ultimate bending moment predicted by those two available models and the newly derived model (Eq. (8)), compared with experimental results.

From Table 2, it can be observed that the present prediction (Eq. (8)), Elchalakani's and Ueda's formulae overestimate the ultimate bending moments by 1.7%, 8.7%, and 11.8%, in average, respectively. The present study, which has included the curvature into account, seems to give more accurate results compared to experiments and other two predictions. However, it still overestimates the ultimate moment, especially for high D/t tubes. This may be explained that, for tubes with high D/t ratios, the plasticity does not spread linearly along the whole circumference as it is assumed in the analysis. In contrast, the plasticity tends to concentrate at the plastic hinge region and causes premature failure.

Considering the coefficient of variation shown in the last row of Table 2, it indicates that the present prediction provides the results with slightly higher degree of variation than that of Elchalakani's but less than that of Ueda's results.

4.2. Comparison of theoretical moment–rotation angle history with experimental results

Figs. 5(a)–(f) show the moment–rotation angle relationship analyzed in this paper compared to experimental results. In the elastic regime, the theoretical moment–rotation curves lie above the experimental results of every case. This may be because of the effect of flow stress. Kim [8] suggested to use lower flow stress for relatively thin sections and used a higher flow stress for relatively thick sections. However, this study assumes the flow stress as σ_y for every calculation. In phase 2, the ovalisation regime, the theoretical curves are constant while the experimental curves slightly increase as the ovalisation progresses. This is due to the effect of strain hardening of material. Considering on phase 3, the structural collapse, the theoretical curves lie slightly above the experimental results, especially at large deflection of tubes. This is because the model does not consider the softening due to the formation of plastic hinges.

Fig. 4. The experimental setup undeformed and deformed specimen in various views: (a) the experimental setup, (b) undeformed tube (UB1) in place, (c) starting in to deform, (d) plastic zone in deformed tube, (e) final deform (side view) and (f) final deform (plain view).

Table 2
Comparison of ultimate moments predicted from simplified model and test results..

Specimen no.	D/t	Experimental ultimate moment	Predicted ultimate moment, Eq. (8)		Elchalakani's ultimate moment, Eq. (4)		Ueda's ultimate moment, Eq. (3)	
		M_{Exp} (kN m)	M_u (kN m)	M_u/M_{Exp}	M_u (kN m)	M_u/M_{Exp}	M_u (kN m)	M_u/M_{Exp}
UB1	21.16	3.20	2.83	0.88	3.02	0.94	2.93	0.92
UB2	25.65	1.85	1.87	1.01	2.12	1.15	2.10	1.13
UB3	26.03	1.12	1.05	0.94	1.18	1.05	1.17	1.04
UB4	32.97	1.76	1.76	1.00	2.09	1.19	2.11	1.20
UB5	36.59	1.09	1.22	1.11	1.13	1.04	1.34	1.23
UB6	42.57	2.38	2.76	1.16	2.76	1.16	2.84	1.19
Average				1.017		1.088		1.118
Coefficient of variation				0.093		0.080		0.096

5. Conclusion

This paper provides a theoretical model to predict the collapse mechanism of thin-walled circular tube subjected to pure bending. The collapse mechanism was divided into 3 phases; elastic regime, ovalisation regime, and structural collapse regime. The elementary theory of elasticity was adopted to explain the elastic regime. The effect of curvature was taken into account for the ovalisation phase. This model predicts the ultimate moment accurately, but seems to overestimate for high D/t tubes.

This paper also developed the structural collapse regime by considering the energy dissipation in rolling hinge in the circumferential direction. The analytical moment–rotation curves lie slightly above the experimental results. In general, it could be concluded that the model developed here provides the results that agree reasonably well with experimental results.

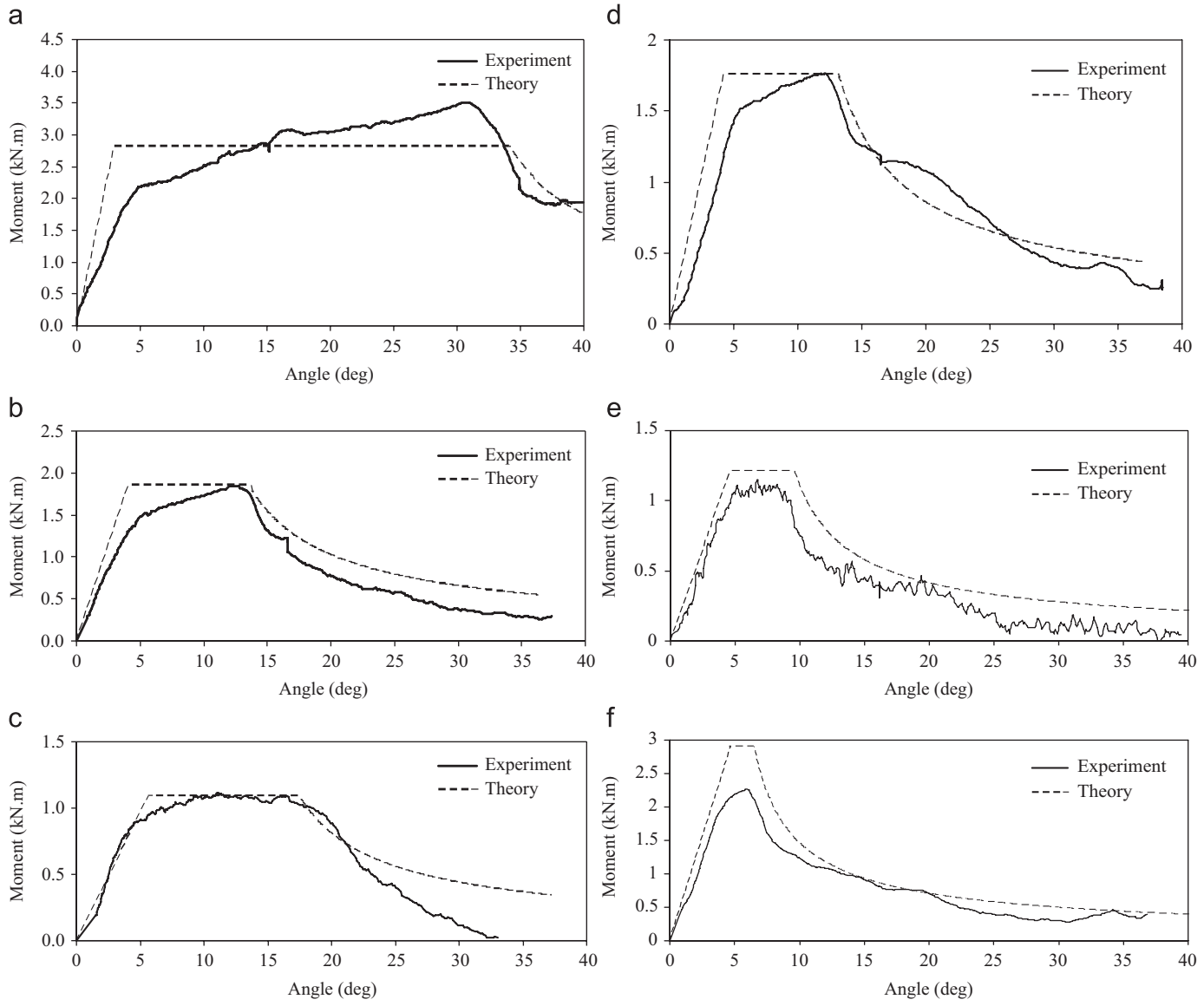

Fig. 5. (a–f) The relationship between rotation angle and bending moment achieved from experiment compared to theoretical analysis. (a) UB1—59.25 × 2.8 ($D/t = 21.16$), (b) UB2—59.0 × 2.3 ($D/t = 25.65$), (c) UB3—46.85 × 1.8 ($D/t = 26.03$), (d) UB4—59.35 × 1.8 ($D/t = 32.97$), (e) UB5—58.55 × 1.6 ($D/t = 36.59$) and (f) UB6—74.50 × 1.8 ($D/t = 41.38$).

Acknowledgment

Authors wish to thank the Department of Industrial Engineering, Ubonratchathani University for support of the test rig.

Appendix

Following are the details of the moment components given in (36). These formulae were calculated by using the numerical techniques and Mathcad [15]:

$$M_1 = \left(\frac{(-1/4)((-R+r)/r)M_0(\pi/R)t\sqrt{2}\phi}{\rho}\right)$$

is a moment component for the crushing of ring.

$$M_2 = \left(\frac{5\times 9\times 10^{-2}((-R+r)^2/(R^2H)M_0 t\phi^3}{\rho}\right)$$

is a moment component for the central hinge.

$$M_3 = \left(\frac{(1/32)(\sqrt{2}/R^2)(R-r)M_0 t\phi}{\rho}\right)$$

is a moment component for the oblique hinge.

Here H and r can be determined from Eqs. (35) and (36), respectively. $M_0 = 4\sigma_0 R^2 t$, t is the thickness of tube, R is the outside radius of tube, ϕ is the mechanism angle of tube (see Eq. (13)), and ρ is the bending rotation at the end of tube, as shown in Fig. 2(b).

References

[1] Kecman D. Bending collapse of rectangular and square section tubes. Int J Mech Sci 1983;25(9–10):623.
[2] Zhang LC, Yu TX. An investigation of the brazier effect of a cylindrical tube under pure elastic–plastic bending. Int J Press Vessels Pip 1987;30:77–86.
[3] Wierzbicki T, Bhat SU. Initiation and propagation of buckles in pipelines. Int J Solids Struct 1986;22(9):985–1005.

[4] Wierzbicki T, Suh MS. Indentation of tubes under combined loading. Int J Mech Sci 1988;30(3–4):229–48.
[5] Cimpoeru SJ, Murray NW. The large-deflection pure bending properties of a square thin-walled tube. Int J Mech Sci 1993;35(3–4):247–56.
[6] Wierzbicki T, et al. Stress profile in thin-walled prismatic columns subjected to crush loading—II. Bending. Comput Struct 1994;51(6):625–41.
[7] Wierzbicki T, Sinmao MV. A simplified model of brazier effect in plastic bending of cylindrical tubes. Int J Press Vessels Pip 1997;71:19–28.
[8] Kim TH, Reid SR. Bending collapse of thin-walled rectangular section columns. Comput Struct 2001;79:1897–991.
[9] Elchalakani M, Zhao XL, Grzebieta RH. Plastic mechanism analysis of circular tubes under pure bending. Int Mech Sci 2002;44:1117–43.
[10] Elchalakani M, Grzebieta RH, Zhao XL. Plastic collapse analysis of slender circular tubes subjected to large deformation pure bending. Adv Struct Eng 2002;5(4):241–57.
[11] Ueda S. Moment–rotation relationship considering flattening of pipe due to pipe whip loading. Nucl Eng Des 1985;85:251–9.
[12] Elchalakani M, Zhao XL, Grzebieta RH. Plastic slenderness limits for cold-formed circular hollow sections. Aust J Struct Eng 2002;3(3):127–41.
[13] Elchalakani M, Zhao XL, Grzebieta RH. Bending tests to determine slenderness limits for cold-formed circular hollow sections. J Constr Steel Res 2002;58:1407–30.
[14] British standard. Tensile testing of metallic materials.1990.
[15] Mathcad 2000. User's Guide, Math Soft, Inc.